Nuclear Instruments and Methods in Physics Research B 574 (2026) 166088

Contents lists available at ScienceDirect

Nuclear Inst. and Methods in Physics Research, B

journal homepage: www.elsevier.com/locate/nimb

A flexible and upgradable parametrization of the electronic stopping cross section☆

Johan Meersschaut [a,b,*], Simon Meersschaut [a]

[a] imec, Kapeldreef 75, 3001 Leuven, Belgium
[b] Department of Physics and Astronomy, KU Leuven 3001 Leuven, Belgium

ARTICLE INFO

Keywords:
Electronic stopping cross section
Stopping power
Parametrization
Double-Konac

ABSTRACT

The stopping cross section describes the characteristic energy loss of fast propagating ions in matter, knowledge of which is important for applications like ion implantation, ion beam analysis, or radiation therapy. When the propagating ions have energies between around 10 keV/u and 10 MeV/u, the energy loss is dominated by the energy transfer to the electrons in the target. In this work we propose to parametrically describe the electronic stopping cross section by using the double-Konac (dK) expression. We present parameter sets for this mathematical model that allow the reproduction of the stopping cross sections of the PSTAR and ASTAR tabulations, of SRIM-2003, and of the ESPNN implementation. In addition, we present parameter sets which account for the experimental data that are published until 2025. We present a parameter set for targets in the gas phase and one for targets in the solid phase.

1. Introduction

The study of the energy loss of ions propagating in matter is crucial for advancing various fields such as ion implantation, ion beam analysis, nuclear physics, outer space exploration, and radiation therapy [1]. The rate of energy loss of an ion per unit path length normalized to the atomic density is called the stopping cross section and may be expressed in units of 10^{-15} eV·cm^2. The stopping cross section depends on the velocity or kinetic energy of the moving projectile (Z_1 and M_1 denoting the atomic number and mass of the projectile) and on the type of target atoms (Z_2, M_2). At projectile kinetic energies below several keV/u, there is considerable energy loss by the interaction of the moving ion with the screened nuclei in the target, known as nuclear energy loss [2]. At projectile energies between 10 keV/u and 100 MeV/u, the energy loss is dominated by interactions of the moving ion with the electrons in the target, referred to as electronic energy loss. At energies above 1 GeV/u and for light projectiles like electrons or positrons, the radiative energy loss becomes increasingly appreciable [3]. In the present study we concentrate on the parametrization for the electronic energy loss.

Multiple analytical theoretical studies have addressed the electronic stopping cross section (ε) of energetic ions in matter. It is found by Lindhard, Scharff and Schiøtt, and by Firsov that at low kinetic energies ($v < \upsilon_0 \cdot Z_1^{2/3}$ with v the speed of the particle and υ_0 the Bohr velocity) the electronic stopping cross section is nearly proportional to the velocity [4–8]. At intermediate energies, the electronic stopping cross section reaches to a maximum, which is referred to as the Bragg peak [9,10]. At higher energies, when the projectiles have velocities higher than the intrinsic velocities of the electrons in the target, the stopping cross section decreases with a dependency as formulated by Bethe,

$$\varepsilon \sim \frac{1}{m_e v^2} \ln\left(\frac{2 m_e v^2}{I}\right)$$

wherein m_e is the electron mass and the material is described by a single parameter, the mean excitation energy I [11,12]. Various refinements to the Bethe theory are known as the Bloch [13,14], shell [15,16], density [17], Lindhard-Sørensen [18], and Barkas correction [19,20]. The high-energy regime of the electronic energy loss is comprehensibly treated in various works (see references [12,16,21–23]).

With the increasing availability of computers, also advanced fundamental computational methods were used to study the electronic stopping cross section. There are various approaches:

- A first class of methods is the non-empirical computational generalization of Bohr's classical stopping model, thus evaluating the

☆ This article is part of a special issue entitled: '2025 IBA – PIXE' published in Nuclear Inst. and Methods in Physics Research, B.

* Corresponding author at: imec, Kapeldreef 75, 3001 Leuven, Belgium.
E-mail address: johan.meersschaut@imec.be (J. Meersschaut).

https://doi.org/10.1016/j.nimb.2026.166088
Received 12 December 2025; Received in revised form 2 March 2026; Accepted 10 March 2026
Available online 21 March 2026

ion–electron interactions as *binary collisions*. An example for this approach is the work of Sigmund and Schinner [24,25], distributed and known as PASS.

- A second approach is using the convolution approximation to model energy-loss processes in matter, as developed by P. Grande *et al.* in the software code CasP [26–28]. CasP explicitly treats situations where the projectile charge state is not fixed, and therefore incorporates the mechanism of *charge-exchange* processes.
- A third class of modern computational studies uses the *dielectric* formalism to theoretically calculate electronic stopping cross sections. Fermi [29] and Lindhard [30] established the groundwork for this formalism. Ziegler demonstrated that Lindhard's dielectric formalism in combination with the local density approximation yields a high-energy behavior in line with the Bethe theory and agreeing with experiments, but it fails at lower energies [31]. A better agreement with experiments down to lower energies is obtained when the dielectric formalism is used with the inclusion of the effects of charge-exchange processes and electron-cloud polarisation of the projectile; see for example the work of de Vera *et al.* [32].
- Finally, one may use first-principles calculations to calculate the electronic stopping. Notably, time-dependent density functional theory allows for a quantitative calculation of the stopping cross section without assumptions about the dielectric function [33–36]. For now, the application of time-dependent density functional theory is still limited due to the high computational cost.

It is commonly accepted that the theoretical considerations give a good account of the physical phenomena that contribute to the electronic energy loss. However, as concerns the computational approaches it is still necessary to confront the results with experimental data to learn about the effect of the chosen approach on the absolute accuracy and precision. As concerns the analytical theories, they can reproduce the overall trends, but they need to be adapted to experimental data by adjusting the model parameters to obtain accurate values. This is the case in the extremely low energy regime where non-linear screening and band-structure effects may be present [37–44]. In addition, it is important to guide the models using experimental data in the transition between extremely low energies and intermediate energies, and at intermediate projectile velocities around the Bragg peak, due to the complex interactions of the moving ion with the electrons in the target [15,45–47]. Finally, the mean excitation energy, which is used in the analytical models to estimate the stopping cross section at high projectile velocities, is often derived from experimental data.

For practical applications one needs a compilation which readily yields the numerical value of the stopping cross section for a given projectile and target. A first successful generalizing implementation is PSTAR/ASTAR, tabulating the stopping cross section for light projectiles in elementary materials as a function of the projectile energy [46]. It is based on estimating the exponent at low energies and the mean excitation energy at high energies from experiments, and on implementing a smooth transition from the low energy to the high energy regime. The PSTAR and ASTAR tables relate to PASS [24,25,48]. The PSTAR/ASTAR compilation only covers the combinations of projectiles and target materials for which experimental data were available at the time of the development.

A second renown implementation to obtain a numerical estimation of the stopping cross section is SRIM. At the basis of SRIM is the work of H.H. Andersen and J.F. Ziegler on the stopping cross section of hydrogen in all elements [49]. The seminal work describes the fitting of experimental data to find the exponent at low energies (proportional to $E^{0.45}$) [50], and on fitting experimental data to find the mean excitation energy and the shell corrections at high energy. Interpolation was used for elements without experimental data and the smooth transition from the low energy to the high energy regime was realized with the formula proposed by Varelas and Biersack [51]. In a subsequent work, J.F. Ziegler combined the stopping cross section for hydrogen and helium projectiles by invoking the concept of an *effective charge* for He, which is dependent on the velocity but not on the target [52]. In 1985, J.F. Ziegler, J.P. Biersack and U. Littmark presented a unified approach to calculate the electronic stopping cross section for all projectiles in all elements [31]. For medium velocity projectiles heavier than helium this involved a multivariant error minimization of the empirical parameters '*effective charge*' and '*screening length*' as a function of the scaled energy. The concepts behind the empirical correction factors were the same as those theoretically predicted by Brandt and Kitagawa [53]. SRIM is recognized for its versatility and ability to produce values that closely match experimentally measured stopping cross sections. For information about the most recent version of SRIM (2003) we refer the reader to [54–56].

The above-mentioned semi-empirical compilations marked a considerable progress towards the parametrization of the stopping cross section. However, due to the absence of recent updates to the parametrizations, researchers were hindered to benefit from the many high-quality experimental data that have been collected in the past decades [57,58]. The scientific community recognized that the stopping cross section needs to be known better, as an error on the stopping cross section adversely affects and often dominates the uncertainty on the modelling of ion implantation, ion beam analysis and clinical proton radiotherapy [59–69].

In recent years researchers have applied machine-learning algorithms to realize a more up-to-date and comprehensive description of the stopping cross section. The studies that are known to the authors are:

- The work of Parfitt and Jackman [70]. The authors trained a random forest regression algorithm using the experimental data of Helmut Paul's stopping power database. The authors demonstrated that the model could make low-error predictions on unseen test data.
- The DL-ESP model, developed by Guo *et al.* [71]. The model is a deep neural network which is trained using the combination of values from the IAEA database and of boundary points in the low-energy regime (E_k/m_a = 1 to 10 keV/u) from the Lindhard-Scharff-Schiøtt model [5]. The DL-ESP predictions are available as numerical tabulations in the supplementary material of the publication by Guo et al. [71].
- ESPNN, which refers to the work of Bivort Haiek *et al.* [72] in which a neural network is trained using experimental values from the IAEA database. The trained neural network is available as a software package.
- The work of Akbari *et al.* [73]. It describes the approach of using five different machine learning models as a base and meta learners to construct a "stacking ensemble machine learning" (S EML) algorithm.
- The ESCS database built by Cheng *et al.* [74]. The authors used an algorithm to build a machine learning database with a minimum number of key descriptors which mimic the low- and high-energy trends. The authors did not use experimental data as input, but instead used values generated by the existing tabulations of SRIM [55], PASS [24], and CasP [27,28].

Common to the studies is that no prescribed theory-inspired energy dependency of the stopping cross section needed to be assumed. The studies are based on refining a model by exposure to a large collection of numerical values.

While the trained neural networks can reach to a good accuracy, their adoption in practical applications is limited. One obstacle to use the different compilations for the stopping cross section is that each compilation requires a different implementation. Therefore, we present a new parametrization for which the coefficients can be traceably updated while the implementation remains unchanged.

2. The dK-parametrization

The sought parametrization for the electronic stopping cross section should be capable of reproducing the existing compilations. There are already multiple parametrizations presented in the literature: Ziegler *et al.* [31,75], Plompen *et al.* [76], and Konac *et al.* [77]. However, the available parametrizations do not have enough degrees of freedom to faithfully reproduce the various existing tabulations and experimental trends. Therefore, we propose a new mathematical model, called the double-Konac (dK) expression, to parametrize the stopping cross section. With the energy $x = E_1/m_a$ in units of MeV/u, we write:

$$\varepsilon(x) = f_1 \bullet KKK_a + f_2 \bullet KKK_b \tag{1}$$

$$with \begin{cases} KKK_a = x^s \bullet \dfrac{\ln(e + p \bullet x)}{(a_0 + a_1 \bullet x^{0.25} + a_2 \bullet x^{0.5} + a_3 \bullet x^{(1+s)})} \\ KKK_b = x^q \bullet \dfrac{\ln(e + r \bullet x)}{(b_0 + b_1 \bullet x^{0.25} + b_2 \bullet x^{0.5} + b_3 \bullet x^{(1+q)})} \end{cases}$$

The expression retains the correct asymptotic behavior at low and high energies, and it also allows to re-use the stopping cross sections of Konac *et al.* [78] by setting $f_1 = 1$ and $f_2 = 0$. It is discussed in [77] how the various coefficients influence the functional behavior of the electronic stopping cross section in the different energy regimes.

The double-Konac expression has ample free parameters to flexibly describe the energy dependence of the stopping cross section [79]. The inclusion of an additional Konac function may lead to overfitting, meaning that an unphysical behavior is obtained. We have inspected most of the optimized curves and rejected the proposed fit if it gave two maxima. During the presented work, we had to reject the proposed solution only twice. In the two cases, re-doing the fit yielded a curve with a single maximum. Apart from the two cases no manual intervention was needed, which reflects the high robustness of the parametrization.

We propose to share the parameters in a json-compatible file in which the parameters are listed in the following order: f_1, s, p, a_0, a_1, a_2, a_3, f_2, q, r, b_0, b_1, b_2, b_3. For each combination of projectile and target material, the file contains both the parameters as well as the estimated relative uncertainty per decade. The relative uncertainty is given as a series wherein the n^{th} value relates to the n^{th} decade, being the interval between $10^{(n-1)}$ keV/u and 10^n keV/u.

The parameters of equation (1) can be chosen, for example, to fit an existing tabulation. Here, we find the parameters to reproduce the output of PSTAR-ASTAR, of SRIM, and of ESPNN. The optimization is achieved by using the differential evolution algorithm from the scipy.optimize library in python [80]. The used cost function is the sum of the squared residuals (χ^2) between the dataset and the calculated stopping cross section:

$$\chi^2 = \sum_{i=1}^{N} \left(\varepsilon_i^{dataset} - \varepsilon_i^{Eq.1}\right)^2,$$

where $\varepsilon_i^{Eq.1}$ means the evaluated stopping cross section according to Eq. (1), and N denotes the number of values in the dataset. The χ^2 cost function is selected here as it proved to work well to fit the stopping cross section around the Bragg peak.

In the context of stopping cross sections one often uses the absolute percentage error $\left|\varepsilon_i^{dataset} - \varepsilon_i^{Eq.1}\right| / \varepsilon_i^{dataset}$ as a metric to compare a compilation to experimental data [70–72,81]. We have also monitored this metric while investigating the various optimizations, even though it was not used in the fitting process. The mean absolute percentage error (MAPE) is defined as:

$$MAPE = \frac{100}{N} \sum_{i=1}^{N} \frac{\left|\varepsilon_i^{dataset} - \varepsilon_i^{Eq.1}\right|}{\varepsilon_i^{dataset}}$$

Besides of the comparison with experimental data, one can also use the MAPE to compare a double-Konac parametrization with a known database. To assess the MAPE with respect to a database, in the present work the value is calculated from an energy eighty times smaller to fifty times larger than the energy of the Bragg peak.

In the following we present various parameter sets. We first describe the parametrization of existing compilations. Further, we also present a parametrization which combines SRIM-2003 with experimental stopping power data that appeared in the literature between the years 2003 and the end of 2024.

3. Parametrization of PSTAR and ASTAR

The PSTAR and ASTAR compilations describe the stopping cross section in various materials as a function of the energy of proton and alpha projectiles, respectively. The compilations were developed by the members of a committee sponsored by the International Commission on Radiation Units and Measurements (ICRU). The scientific approach behind the databases is described in reports that are coordinated by Bichsel [46] and Berger [21]. The ICRU committee has given much effort to estimate the mean excitation energy which is used in the Bethe theory for the calculation of the stopping cross section at high energies [82]. Subsequently, the experimental stopping powers at low energy together with the estimated values from the Bethe theory at high energies are fitted by a cubic spline function for the interpolation around the Bragg peak.

Estimations for the stopping cross section according to PSTAR and ASTAR are available as a web-service [82]. We have used this web-service to download tables of stopping cross sections in various elementary materials. Note that this compilation only covers proton and alpha particles as projectiles and not the full list of elementary target materials. We show in Fig. 1 two examples of the stopping cross section which are derived from PSTAR and ASTAR, namely for H in Cu and for He in Fe.

The red curves in Fig. 1 represent the best fits to the data, illustrating that Equation (1) allows one to reproduce the tabulations of PSTAR and ASTAR faithfully. The red curves are the sum of the two terms in Equation (1) that are shown explicitly as a green and a blue curve. We could not recognize any systematic trend in the role of the two terms: sometimes the two terms are each dominant in either the low- and high-energy domain, sometimes they contribute comparatively near the Bragg peak, and for other projectile-target combinations only one term is significant. Remarkably, for all combinations a good fit was found, as is also reflected by the low MAPE values. We refer to this as the (SCS-1993)-parametrization.

4. Parametrization of SRIM-2003

SRIM has a vast history related to describing the stopping cross section of energetic ions in matter. The stopping cross section is based on the near-velocity proportional behavior at low energy and the Bethe behavior at high energy. In addition, it foresees in a smooth transition by interpolation from the low energy to the high energy regime [51,83]. A unique feature of SRIM is that it contains a scaling formalism to calculate the electronic energy loss cross section of heavier projectiles based on the behavior for light ions in the same medium [31]. The first consideration for this is that the Bethe formula contains a factor which is proportional to the square of the atomic number of the projectile, Z_1^2. The second consideration is the assumption that a heavy projectile loses part of its electrons which are moving slower than the relative velocity between the ion and the target, and it is implemented through the concept of a fractional effective charge. The effective charge of a heavy ion is assumed to be velocity-dependent, though not target-dependent. For details and practical examples, we refer to the works of Ziegler and Manoyan [84], and to Rauhala and Ziegler [85]. The implementations in SRIM-1995 and SRIM-1998 are known and are adopted in various other software packages (see for example SIMNRA [86], IBA-

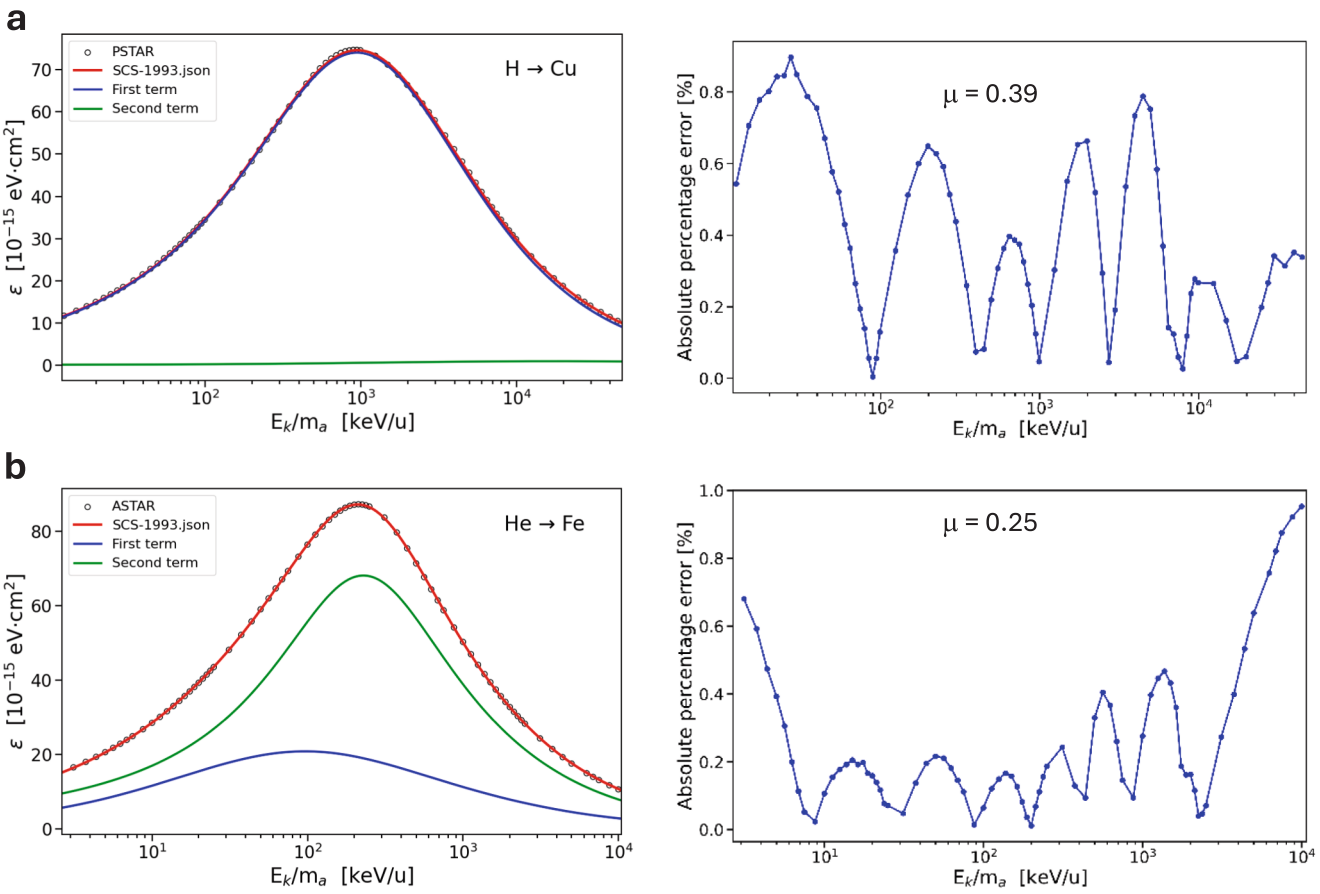

Fig. 1. Comparison between PSTAR-ASTAR and the dK-parametrization for the examples of (a) hydrogen projectiles in copper and (b) helium projectiles in iron. Left: the stopping cross section. The black symbols are from PSTAR and ASTAR, the red curve shows the SCS-parametrization. The horizontal axis is the kinetic energy of the projectile divided by its atomic mass. The two terms of Equation (1) are shown as the green and blue lines. Right: the absolute percentage error as a function of the scaled kinetic energy. The mean absolute percentage error is indicated.

DataFurnace [87], Ruthelde [63], and MC-ERD [88]).

In later releases of SRIM the implementation was further improved to reproduce the experimental results more closely. The calculated stopping cross section differs between SRIM-1998 and SRIM-2003, especially for projectile-target combinations that had received attention at the time. Thus, the parametrization of SRIM-2003 implied a significant improvement in the accuracy in relation to the experimentally measured stopping cross sections [55,56]. On the other hand, the developers of SRIM-2003 have chosen to modify the underlying parametrization, and the implementation is not publicly disclosed. Thus, to use the stopping cross sections of SRIM-2003 one necessarily must run the SRModule.exe of SRIM on a Windows machine and generate a collection of files that contain the stopping power as a function of energy. Also note that we found no difference in the stopping cross sections between SRIM-2003 and the more recent releases of SRIM, like SRIM-2013.

The results reported here are based on the stopping cross sections of SRIM-2013.00 [89]. The stopping cross section as a function of energy for the interval between 0.001 MeV and 5000 MeV for the 92 x 92 combinations of projectiles and targets are extracted from SRIM and saved in separate text files. Since SRIM gives a different output for certain elementary targets depending on whether the target is indicated to be either a gas or a solid, we have saved the outputs for the gas and the solid state separately.

The output of SRIM for a selection of projectiles and targets is shown as datapoints in Fig. 2. Fig. 2 also shows the best fit using Eq. (1). It is seen that the proposed analytical expression reproduces the electronic stopping cross section well, while the fitting with a single Konac function led to notable deficiencies especially at low energies. The panels on the right in Fig. 2 visualize the absolute percentage error between the SRIM output and the dK-parametrization. One notices that the percentage error tends to be larger at both low and high energies. This behavior is as expected, since the squared residuals were minimized, and a comparable squared residual will lead to a larger percentage error when the value is smaller.

The performance of the fitting for the different projectile-target combinations and a statistical analysis of the fit quality is shown in Fig. 3. The fit quality for the stopping cross section for H- and He-projectiles is particularly good and comparable with the quality of the (SCS-1993)-parametrization. The average MAPE for the 92 x 92 combinations is 0.83%, which is still much smaller than the uncertainty on the SRIM parametrization. For those cases where the MAPE is larger than 1% it is associated with unexpected, peculiar features of the stopping cross section at low or at high energy obtained from SRIM.

For SRIM-2003, Ziegler *et al.* [90] obtained a mean absolute percentage error of 4.6% while considering over 25 000 points, whereas Helmut Paul reported a mean absolute percentage error $\Delta_{abs} \pm \sigma$ of (5.3 $\pm$ 7.1) % with 22 000 experimental points [81]. Thus, the deviation of the current parametrization from SRIM is approximately five times smaller than the uncertainty on SRIM, and the contribution to the uncertainty of the new parametrization is negligible. Considering that the dK-parametrization does not significantly add to the uncertainty, we pragmatically estimate the uncertainty related to this parametrization for all energy intervals as 5%.

Note that the dK-parametrization also allows the reproduction of detailed features which have been studied. For example, in certain cases the most probable method of energy loss is not ionization or excitation,

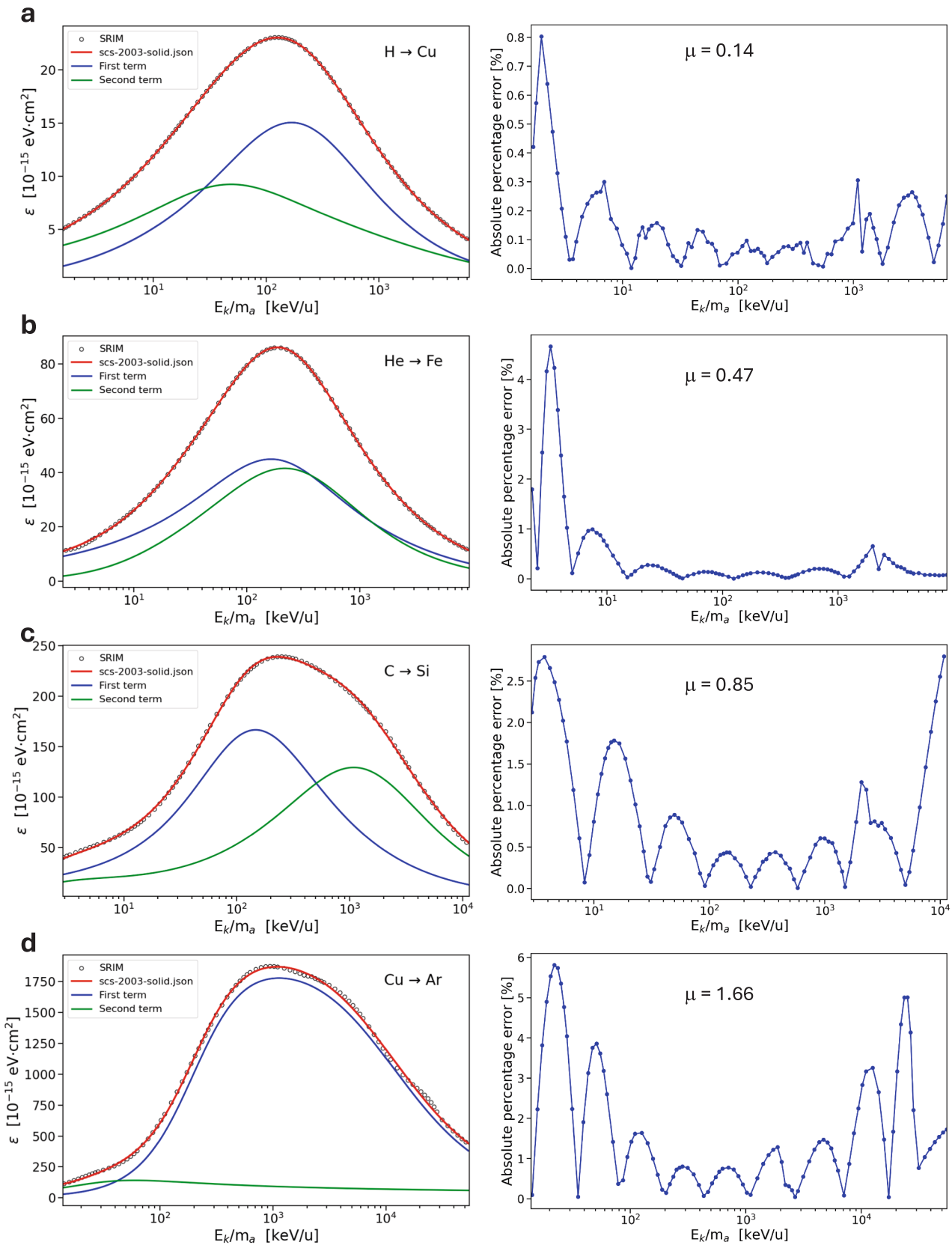

Fig. 2. Left: Comparison between SRIM (black symbols) and the fit according to (SCS-2003-solid) for a selection of projectiles and target elements. The horizontal axis is the kinetic energy of the projectile divided by its atomic mass. The contributions of the two terms of Eq. (1) are shown separately. Right: absolute percentage error between the SRIM output and the fitted parametrization. The reported value of μ is the mean absolute percentage error.

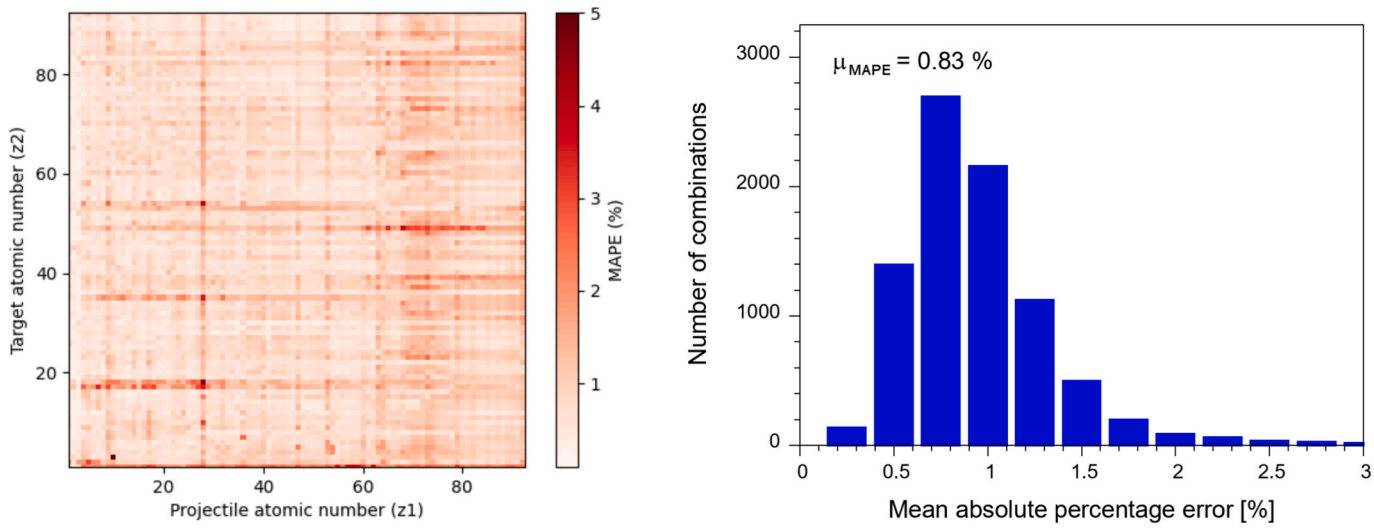

Fig. 3. Distribution of the absolute percentage error for the (SCS-2003-solid)-parametrization compared to SRIM.

but charge exchange. For H → He, this leads to a deviation from linear dependency of the stopping cross section on the projectile velocity around the threshold energy of approximately 20 keV [91,92]. The threshold is implemented in the SRIM-2013 code and is properly reproduced here in the present parametrization with Equation (1). The non-linearities for the stopping of low-velocity projectiles in solids caused by charge-exchange and density of states as discussed in the introduction were reported after the release of SRIM-2003 [37–44]. Thus, these features are not reflected in SRIM and therefore also not in the present parametrization.

A separate note goes to the difference between materials in the solid and in the gas phase. Indeed, there is experimental evidence that the stopping cross section differs depending on the state of matter. We refer the reader to the works of Ziegler *et al.* [93] and of H. Paul [81]. To illustrate the importance with an example, notice that the stopping cross section in an oxygen target is conventionally determined in the gas state, while the oxygen in a silicon-oxide sample should be considered as in the solid state. In SRIM a different stopping cross section for the gas and the condensed phase is implemented for the following elemental targets: H, N, O, F, Cl, Br, and Iodine. We have fitted Equation (1) to the energy dependent stopping cross section of any projectile-target combination and for both the gas- and solid- phases as derived from SRIM. The results are referred to as the (SCS-2003-gas)-parametrization and the (SCS-2003-solid)-parametrization, respectively.

5. Parametrization of ESPNN

As was indicated in the introduction of this article, studies have been published in recent years in which machine learning methods are used to describe the multi-dimensional dependency of the stopping cross section.

ESPNN refers to a recent effort to develop a computational framework for describing the stopping cross section using a neural-network code as realized by Bivort Haiek *et al.* [72]. The authors applied unsupervised machine learning methods to clean the data of the IAEA database (2021) from suspicious outliers and old isolated values in an automated manner before training a deep neural network. The neural network accurately reproduces the training data, comparable to alternative implementations. The ESPNN forward propagation code is available from a public repository [94].

Machine-learning methods are attractive and have complementary value compared to the theory-inspired approaches. We worked with the ESPNN because it is based on the largest number of experimental values, and it is developed without the adoption of a theoretical presumption. In addition, the ESPNN work involved an advanced unbiased density based spatial clustering and filtering of the experimental data. Unfortunately, the package is only functional in the python environment in which it was developed. Therefore, a parametrization with the present framework may secure the work for future usage and facilitate the intercomparison with other databases.

The output of ESPNN for a selection of projectiles and targets, together with the best fit using Eq. (1) is shown in Fig. 4. It is again seen that Equation (1) reproduces the electronic stopping cross section well. We refer to the results as the (SCS-2022)-parametrization.

The MAPE between the ESPNN output and the best fits is mostly between 1% and 2%, which is worse than for SRIM but still better than the difference between ESPNN and the experimental data of around 5%. Therefore, the (SCS-2022)-parametrization may be used as a proxy for ESPNN.

6. The (SCS-2025-gas)-parametrization

In the past, the SRIM software has been the most intensely used approach by researchers to estimate the stopping cross section. Substantial improvements have been implemented in the various releases until SRIM-2003. However, past SRIM-2003, the electronic stopping cross section implementation has remained unchanged; only the binary collision module and the graphical user interface have received updates. The lack of recent updates detracts from the high-quality experimental data that have been collected in the past decades. In the present section we develop a parametrization which accounts for the new experimental data if they are published after 2003 and before 2025. SRIM-2003 is reproduced when no new experimental data are published in this period.

The experimental stopping cross sections are obtained from the IAEA database and filtered on the criterium of whether they were published before or after 2003. Advantageously, the values in the database are linked to the publication in which they appeared, and there is also an uncertainty associated with the various stopping cross section values. The values that appear in the same publication are said to belong to the same dataset. For fitting we use the IAEA datapoints together with the uncertainty published after 2003. The IAEA datapoints are complemented with datapoints generated using the dK-formalism and the (SCS-2003-gas) parameter set. The estimated percentage error for the self-generated datapoints is 5%.

The parameters for the best fit function are found by minimizing the sum of the weighted squared differences between the datapoints and the predictions. The weight ($w_{i,j}$) for a datapoint (j) in a dataset (i) is based on the uncertainty (estimated percentage error) scaled by the square

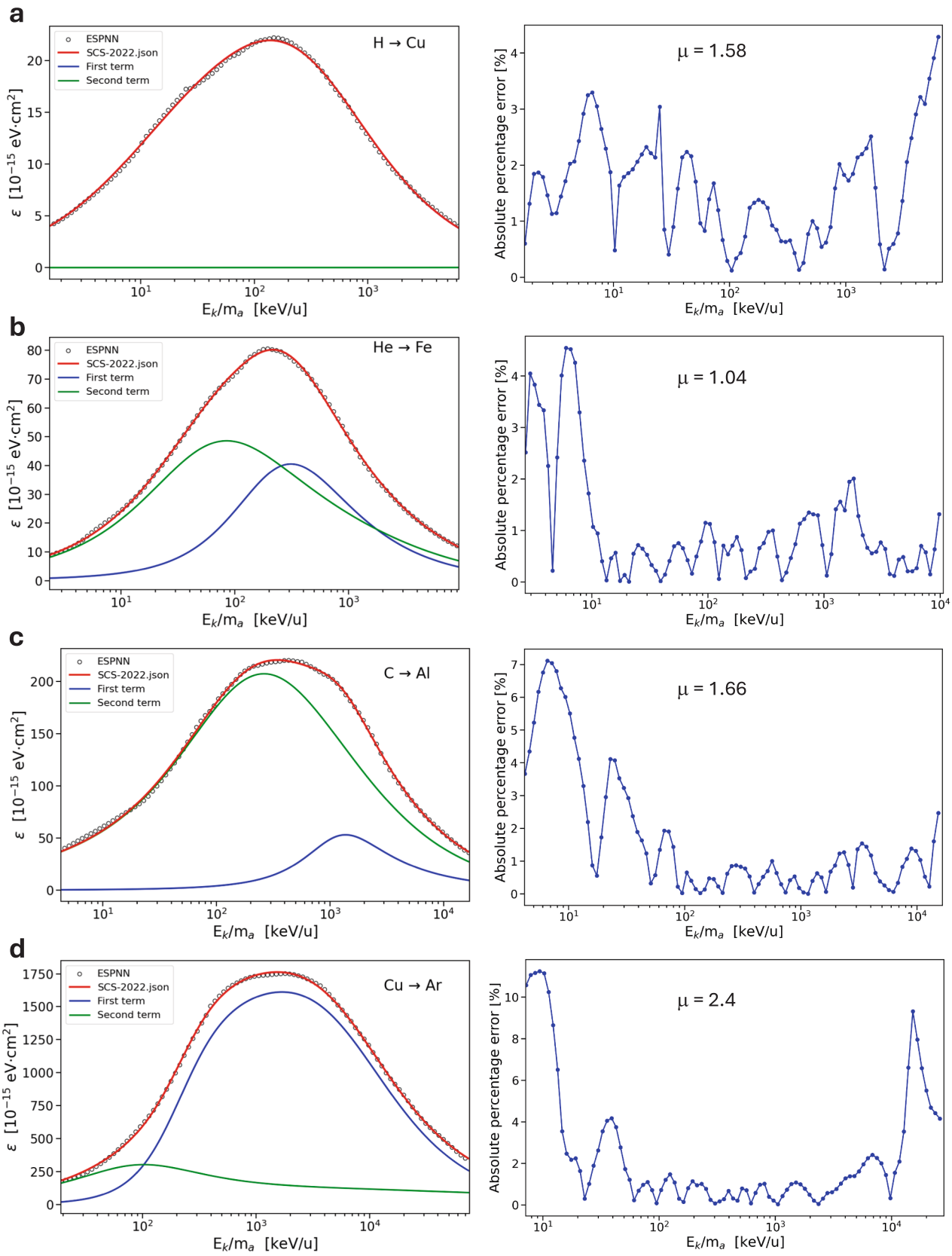

Fig. 4. Left: Comparison between ESPNN (black symbols) and the fit (SCS-2022, red curve), similar as figure 2. The combination C → Si was avoided because it was erroneous. The horizontal axis is the kinetic energy of the projectile divided by its atomic mass. Right: absolute percentage error between the ESPNN output and the fitted parametrization.

root of the number of datapoints in a specific decade for that dataset. This is done to compensate the weight of a dataset with less points compared to one with more points. With this the fitting entails finding the optimal parameter values by minimizing the sum of weighted squared residuals (S):

$$S = \sum_{i,j} \left[w_{i,j} \bullet \left(\varepsilon_{i,j} - \varepsilon_{fit} \right) \right]^2.$$

If no new experimental stopping cross sections since 2003 are reported in the database, then the parametrization returns the trend which was given by (SCS-2003-gas). Otherwise, the curves are refined. This is illustrated in Fig. 5. The literature values published before 2003 are plotted in grey squares, whereas recent experimental values are plotted as blue-coloured diamond symbols. The examples in Fig. 5 illustrate the effect of the new experimental values on the parametrization. For example, the stopping cross section for H projectiles in nitrogen gas is significantly adjusted due to the additional datapoints which were published by Jedrejcic *et al.* [91]. The stopping cross section for He projectiles in Si remains unchanged at energies above the Bragg peak [95] but is slightly modified at medium energies due to the results of Tran *et al.* [96]. The position of the Bragg peak for argon projectiles in silicon is shifted towards higher energies, in accordance with recent experimental results of Javanainen *et al.* [97]. And the stopping cross section for He in Au is enhanced both at medium energies as well as at the Bragg peak.

Not only the values of the stopping cross section are modified, but also updated are the associated estimated uncertainties. The estimated percentage error in each decade is calculated as [98]:

$$\delta = \sqrt{\left(\sum_i \left[{}^1\!/_{\delta_i} \right]^2 \right)^{-1}},$$

whereby for each dataset (i) only one value for the estimated percentage error is considered. If there are for a specific projectile/target/energy-decade combination in the IAEA no new datapoints since 2003, then the self-generated dataset is the only one remaining and the resulting uncertainty is the same as in (SCS-2003-gas).

The effectiveness of the followed approach is illustrated in Fig. 6. It shows the frequency of occurrence of mean absolute percentage error when comparing a given parametrization with the IAEA database. On the left we show the proximity of the parametrization to the data published before and until 2003, while on the right the comparison is made for data that are published after 2003. The histograms on the left (top versus bottom) illustrate that the new parametrization (SCS-2025-gas) has an equivalent performance as compared to (SCS-2003-gas) to the data before 2003. Yet, one concludes from the comparison on the right (top versus bottom) that the new parametrization reflects the experimental stopping cross sections much better than the original one.

7. The (SCS-2025-solid)-parametrization

In the previous sections we mentioned that the stopping cross section in SRIM is treated differently depending on the target being in the gaseous or the solid state. Indeed, the subject was intensely studied experimentally and reviewed by David Thwaites [99] and by Helmut Paul [81]. There appears to be much experimental evidence for a lower stopping cross section in H, N, O, F, Cl, Br, and Iodine targets in the (compound) solid state compared to when the targets are in the gas phase. Note that this appears not to be the case for noble gas targets. For example, no difference in the stopping is found between gaseous and solid argon. The explanation given is that solid argon is a weakly bound van der Waals solid. Instead, the negative effect in other cases is understood as a difference in mean ionization potential between the gaseous and the condensed state. Detailed studies and convincing experimental results were published for oxides and nitrides of metals

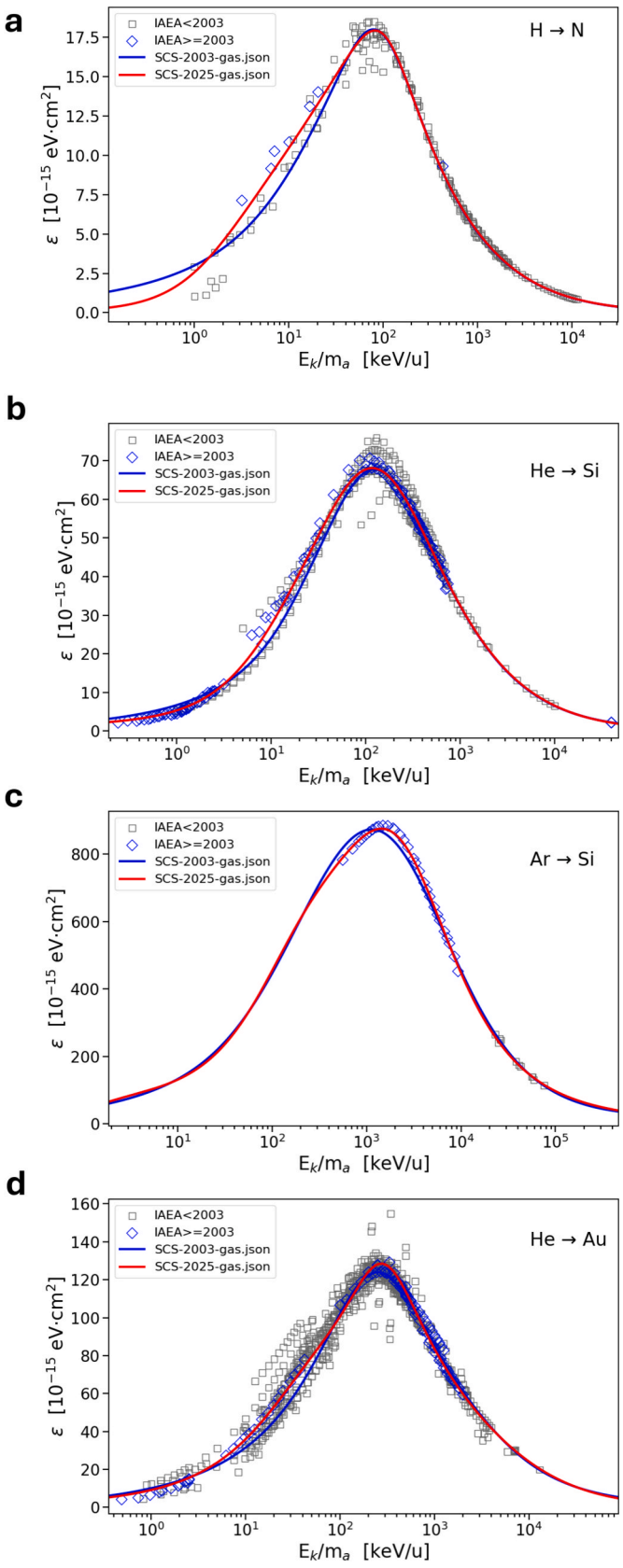

Fig. 5. Stopping cross section for various projectile-target combinations. The literature values are obtained from the IAEA database and sorted according to the date of publication. The blue curves are from (SCS-2003-gas) while the red curves correspond to the (SCS-2025-gas)-parametrization.

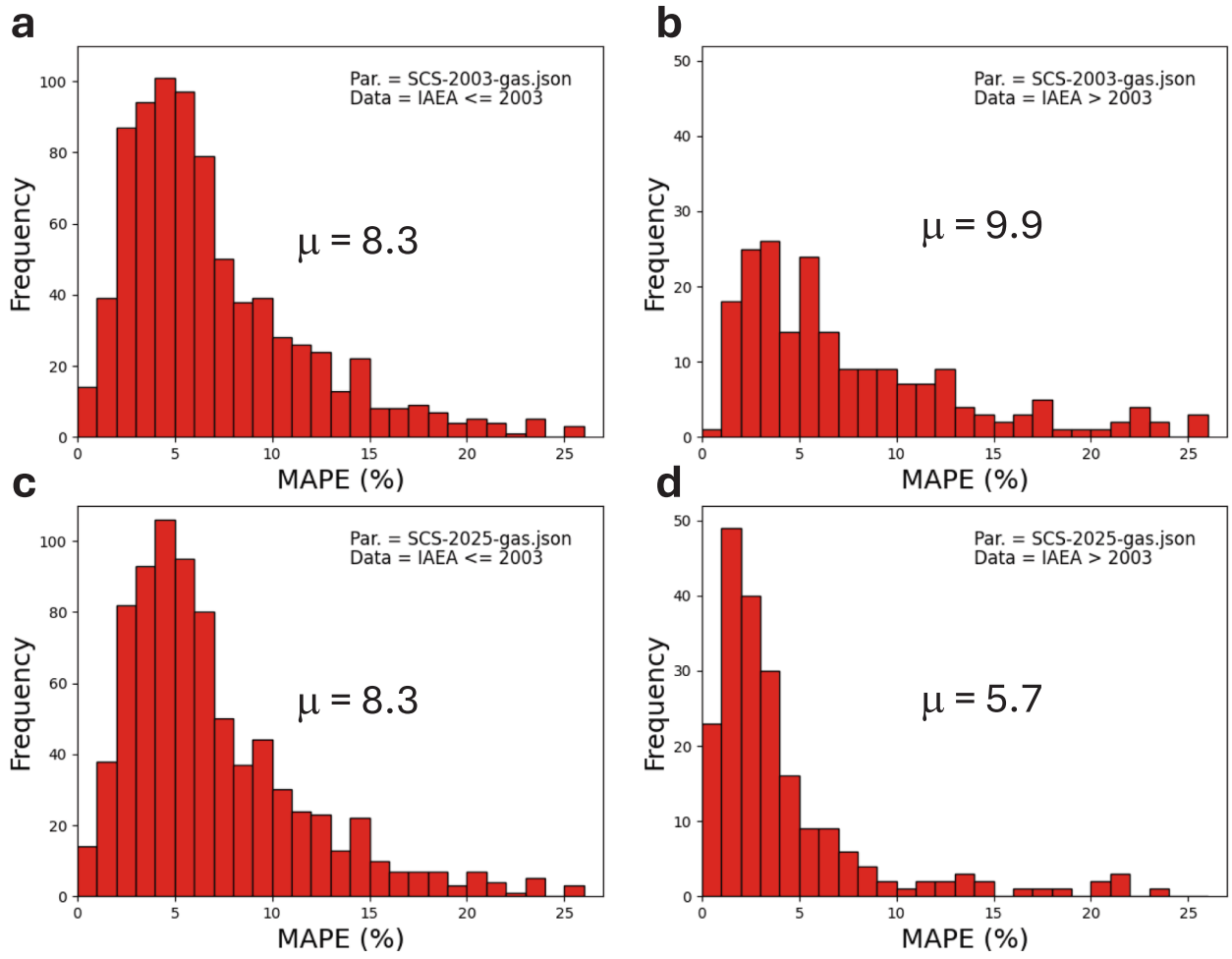

Fig. 6. Histogram showing the frequency of a specific mean absolute percentage error (MAPE) when comparing the parametrization with the IAEA database. One count represents one projectile-target combination. The top row is for the (SCS-2003-gas)-parametrization, while the bottom row is for (SCS-2025-gas). The left column is for the data in IAEA published before 2003, while the panels on the right are for the data that are published after 2003.

and for other organic compounds like pentane, hexane, or alcohol [81]. Similar effects of a reduced stopping cross section were also obtained with real-time density functional theory calculations for protons in various polymers like polyethylene and poly-(methyl methacrylate) [68] and for water in the distinct phases [100].

In the present work we follow the approach of SRIM to reduce the stopping cross section in the solid state in comparison with the gas state. We determined a functional relationship between stopping in gasses and solids by comparing the output of SRIM-2013 for both states. By fitting the ratio of the outputs of SRIM, we found that the reduction factor (r) can be modelled as:

$$r = 1 + 0.087/2 \cdot \{1 - erf((x - 1.05)/0.033)\} \textit{ for hydrogen projectiles},$$

and

$$r = 1 + 0.087/2 \cdot \{1 - erf((x - 0.44)/0.280)\} \textit{ for other projectiles},$$

with the kinetic energy x being the dimensionless value of E_k/m_a when expressed in units of MeV/u and with *erf(x)* denoting the error function. The correction amounts to 8.7% at low energy and vanishes above a characteristic energy which is 1050 keV/u for hydrogen projectiles and 400 keV/u for the other projectiles.

To implement the reduction in the present framework, we have produced numerical output tables for the above-mentioned gasses from the (SCS-2025-gas)-parametrization which we divided by the gas-to-solid reduction factor. These tables are then again fitted to Equation (1) and the result is illustrated in Fig. 7. From Fig. 7 it can be observed that the characteristic energy below which the stopping cross section is reduced for the solid state is different between protons and heavier projectiles, in accordance with the implementation in SRIM-2003. The parameters that reproduce the stopping cross section are saved as (SCS-2025-solid). The uncertainties are taken as identical to the ones for the (SCS-2025-gas)-parametrization.

8. Conclusion

We introduced the double-Konac expression to flexibly model the electronic stopping cross section as a function of energy. The parametrization is shown to be able to reproduce multiple existing tabulations and thereby proves to be a robust framework.

We generated various parameter files that correspond to pre-existing parametrizations. Besides, we developed a parametrization which accounts for the latest experimental stopping cross section measurements. All the parametrizations are publicly available for downloading from https://johan.meersschaut.net/scs/files. The following parameter files are currently available:

- SCS-1993 – reproducing the stopping cross section of ASTAR/PSTAR,
- SCS-2003-gas – corresponding to SRIM-2003 for materials in the gas phase,

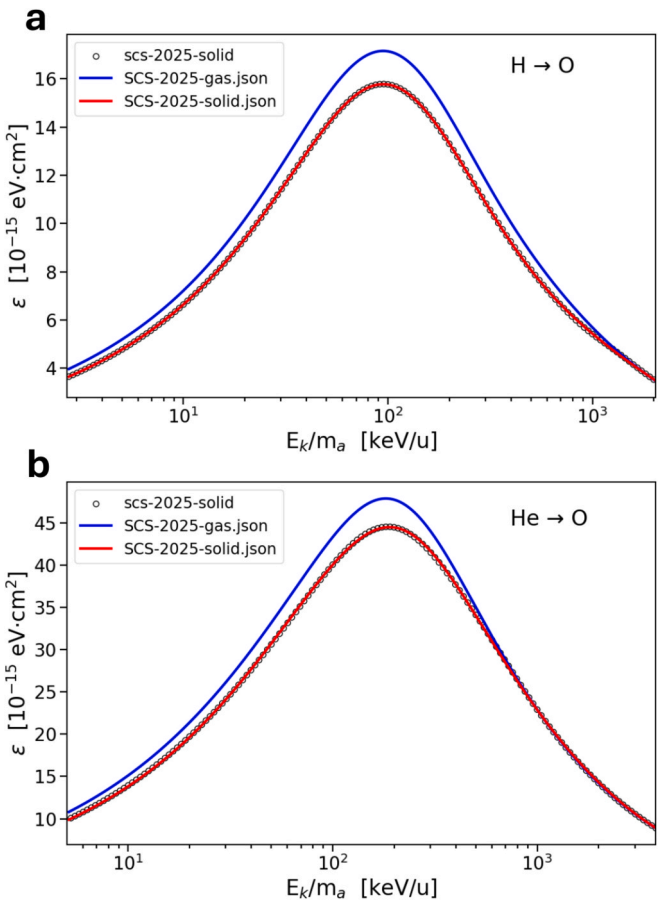

Fig. 7. Estimated stopping cross section for H and He projectiles in oxygen. The blue curve is the (SCS-2025-gas)-estimation. The black datapoints are obtained by application of the reduction factor. The parameters that best describe the reduced stopping cross section are referred to as (SCS-2025-solid).

- SCS-2003-solid – corresponding to SRIM-2003 for materials in the solid phase,
- SCS-2020 – reproducing the stopping cross section of ESPNN,
- SCS-2025-gas – based on (SCS-2003-gas) but including IAEA data until 2025,
- SCS-2025-solid – based on (SCS-2025-gas) but for materials in the solid state.

Given that the various works are now represented in a uniform manner, they are easier to be intercompared. A tool to intercompare the various parametrizations is available at https://johan.meersschaut.net/scs/plot.

It is hoped that continued research will yield additional high-quality experimental values for the stopping cross section [101] which in the future may be used to update the parametrizations. Special attention and detailed studies should aim to clarify the predictive power of the existing parameter sets for the stopping cross section of heavy ions [59] and for light projectiles at extremely low velocities [102]. Also, in-depth studies may focus on a specific projectile-target combination to yield a more accurate parameter set and uncertainty evaluation using the proposed representation. An advantage of the proposed construction is that the parametrization for one specific projectile-target combination can be updated without affecting the other projectile-target combinations.

It is expected that future research will result in new parameter files and, therefore, systematically mentioning the used parameter file when stopping cross sections affect the results will advance the traceability of the research.

Declaration of competing interest

The authors declare that they have no known competing financial interests or personal relationships that could have appeared to influence the work reported in this paper.

Acknowledgements

We thank Ruben Van der Borght (KU Leuven and imec) for extracting the tabulation files from the ESPNN network and Mathias Meersschaut (KU Leuven) for developing and maintaining the web interface.

References

[1] S. Limandri, P. de Vera, R.C. Fadanelli, L.C.C.M. Nagamine, A. Mello, R. Garcia-Molina, M. Behar, I. Abril, Energy deposition of H and He ion beams in hydroxyapatite films: a study with implications for ion-beam cancer therapy, Phys. Rev. E 89 (2014) 022703, https://doi.org/10.1103/PhysRevE.89.022703.
[2] A.N. Zinoviev, P.Y. Babenko, K. Nordlund, Nuclear stopping powers for DFT potentials, Nucl. Inst. Methods Phys. Res. B 508 (2021) 10–18, https://doi.org/10.1016/j.nimb.2021.10.001.
[3] E. Haug, W. Nakel, The elementary Process of Bremsstrahlung, World Scientific, Singapore, 2004.
[4] J. Lindhard, M. Scharff, Energy dissipation by ions in the keV region, Phys. Rev. 124 (1961) 128, https://doi.org/10.1103/PhysRev.124.128.
[5] J. Lindhard, M. Scharff, H.E. Schiøtt, Energy loss in matter by fast particles of low charge, Kgl. Danske Videnskab. Selskab. Mat. Fys. Medd. 22 (1963) 14.
[6] O.B. Firsov, Zh. Eksp. Teor. Fiz. 32, 1464 (1957) (English transl. Sov. Phys. JETP 5, 1192 (1957).
[7] O.B. Firsov, Zh. Eksp. Teor. Fiz. 34,447 (1958) (English transl. Sov. Phys. JETP 7, 308 (1958).
[8] O.B. Firsov, Zh. Eksp. Teor. Fiz. 36, 1517 (1959) (English transl. Sov. Phys. JETP 9,1076 (1959).
[9] W.H. Bragg, R. Kleeman, On the α particles of radium, and their loss of range in passing through various atoms and molecules, Philosophical Magazine Series. 6 (1905) 10:57, 318-340, doi:10.1080/14786440509463378.
[10] P. Sigmund, A. Schinner, Height and position of the Bragg peak in the stopping of charged particles, J. Appl. Phys. 127 (2020) 164302, https://doi.org/10.1063/5.0005292.
[11] H.A. Bethe, Zur Theorie des Durchgangs schneller Korpuskularstrahlen durch Materie, Ann. Physik 5 (1930) 325, https://doi.org/10.1002/andp.19303970303.
[12] F. Salvat, Bethe stopping-power formula and its corrections, Phys. Rev. A 106 (2022) 032809, https://doi.org/10.1103/PhysRevA.106.032809.
[13] F. Bloch, Zur Bremsung rasch bewegter Teilchen beim Durchgang durch Materie, Ann. Physik 16 (1933) 287, https://doi.org/10.1002/andp.19334080303.
[14] F. Bloch, Bremsvermögen von Atomen mit mehreren Elektronen, Z. Physik 81 (1933) 363, https://doi.org/10.1007/BF01344553.
[15] H. Bichsel, Stopping power and ranges of fast ions in heavy elements, Phys. Rev. A 46 (1992) 5761, https://doi.org/10.1103/PhysRevA.46.5761.
[16] J.F. Ziegler, Stopping of energetic light ions in elemental matter, J. Appl. Phys. 85 (1999) 1249, https://doi.org/10.1063/1.369844.
[17] U. Fano, Atomic Theory of Electromagnetic Interactions in Dense Materials, Phys. Rev. 103 (1956) 1202, https://doi.org/10.1103/PhysRev.103.1202.
[18] J. Lindhard, A.H. Sørensen, Relativistic theory of stopping for heavy ions, Phys. Rev. A 53 (1996) 2443, https://doi.org/10.1103/PhysRevA.53.2443.
[19] W.H. Barkas, J.N. Dyer, H.H. Heckman, Resolution of the Σ^- Mass Anomaly, Phys. Rev. Lett. 11 (1963) 26, https://doi.org/10.1103/PhysRevLett.11.26.
[20] J.C. Ashley, R.H. Ritchie, W. Brandt, $Z_1$3-Dependent stopping power and range contribution, Phys. Rev. A 8 (1973) 2402, https://doi.org/10.1103/PhysRevA.8.2402.
[21] M.J. Berger et al., Stopping power and ranges for protons and alpha particles, ICRU Report 49, Journal of the ICRU 25 (1993) 1-68. For the dataset hosted at NIST, doi:10.18434/T4NC7P.
[22] F. Salvat, P. Andreo, SBETHE: stopping powers of materials for swift charged particles from the corrected Bethe formula, Comput. Phys. Commun. 287 (2023) 108697, https://doi.org/10.17632/7zw25f428t.1.
[23] P. Sigmund, Springer series in solid-state sciences 151: Particle Penetration and Radiation Effects (2006); ISBN-10: 3540317139.
[24] P. Sigmund, A. Schinner, Binary stopping theory for swift heavy ions, Eur. Phys. J. D 12 (2000) 425, https://doi.org/10.1007/s100530070004.
[25] P. Sigmund, A. Schinner, Progress in understanding heavy-ion stopping, Nucl. Instrum. Methods B 382 (2016) 15, https://doi.org/10.1016/j.nimb.2015.12.041.
[26] P.L. Grande, G. Schiwietz, The unitary convolution approximation for heavy ions, Nucl. Instrum. Methods Phys. Res. B 195 (2002) 55–63, https://doi.org/10.1016/s0168-583x(01)01164-8.
[27] P.L. Grande, G. Schiwietz, Convolution approximation for the energy loss, ionization probability and straggling of fast ions, Nucl. Instrum. Methods Phys. Res. B 267 (2009) 859, https://doi.org/10.1103/PhysRevA.58.3796.
[28] P.L. Grande, G. Schiwietz, CasP (Convolution Approximation for Swift Particles) program, is available at https://lief.if.ufrgs.br/pub/CasP/ (accessed Dec. 2025).

[29] E. Fermi, The ionization loss of energy in gases and in condensed materials, Phys. Rev. 57 (1940) 485–493, https://doi.org/10.1103/PhysRev.57.485.
[30] J. Lindhard, On the properties of a gas of charged particles, Danske Matematisk-Fysiske Meddelelser 28 (1954) 1–57.
[31] J.F. Ziegler, J.P. Biersack, U. Littmark, The stopping and range of ions in solids, The stopping and ranges of ions in matter Vol. 1 (1985), Pergamon press, New York.
[32] P. de Vera, I. Abril, R. Garcia-Molina, Electronic cross section, stopping power and energy-loss straggling of metals for swift protons, alpha particles and electrons, Front. Mater. 10 (2023) 1249517, https://doi.org/10.3389/fmats.2023.1249517.
[33] J.M. Pruneda, D. Sánchez-Portal, A. Arnau, J.I. Juaristi, E. Artacho, Electronic stopping power in LiF from first principles, Phys. Rev. Lett. 99 (2007) 235501, https://doi.org/10.1103/PhysRevLett.99.235501.
[34] A. Ojanperä, A.V. Krasheninnikov, M. Puska, Electronic stopping power from first-principles calculations with account for core electron excitations and projectile ionization, Phys. Rev. B 89 (2014) 035120, https://doi.org/10.1103/PhysRevB.89.035120.
[35] A. Schleife, Y. Kanai, AA. Correa, Accurate atomistic first-principles calculations of electronic stopping, Phys. Rev. B 91 (2015) 014306, https://doi.org/10.1103/PhysRevB.91.014306.
[36] E.E. Quashie, A.A. Correa, Electronic stopping power of protons and alpha particles in nickel, Phys. Rev. B 98 (2018) 235122, https://doi.org/10.1103/PhysRevB.98.235122.
[37] S.N. Markin, D. Primetzhofer, M. Spitz, P. Bauer, Electronic stopping of low-energy H and He in Cu and Au investigated by time-of-flight low-energy ion scattering, Phys. Rev. B 80 (2009) 205105, https://doi.org/10.1103/PhysRevB.80.205105.
[38] E.D. Cantero, G.H. Lantschner, J.C. Eckardt, N.R. Arista, Velocity dependence of the energy loss of very slow proton and deuteron beams in Cu and Ag, Phys. Rev. A 80 (2009) 032904, https://doi.org/10.1103/PhysRevA.80.032904.
[39] D. Goebl, D. Roth, P. Bauer, Role of d electrons in electronic stopping of slow light ions, Phys. Rev. A 87 062903, doi:10.1103/PhysRevA.87.062903.
[40] D. Goebl, W. Roessler, D. Roth, P. Bauer, Influence of the excitation threshold of d electrons on electronic stopping of slow light ions, Phys. Rev. A 90 (2014) 042706, doi:10.1103/PhysRevA.90.042706.
[41] D. Roth, B. Bruckner, M.V. Moro, S. Gruber, D. Goebl, J.I. Juaristi, M. Alducin, R. Steinberger, J. Duchoslav, D. Primetzhofer, P. Bauer, Electronic stopping of slow protons in transition and rare earth metals: breakdown of the free electron gas concept, Phys. Rev. Lett. 118 (2017) 103401, https://doi.org/10.1103/PhysRevLett.118.103401.
[42] D. Roth, B. Bruckner, G. Undeutsch, V. Paneta, A.I. Mardare, C.L. McGahan, M. Dosmailov, J.I. Juaristi, M. Alducin, J.D. Pedarnig, R.F. Haglund Jr., D. Primetzhofer, P. Bauer, Electronic stopping of slow protons in oxides: scaling properties, Phys. Rev. Lett. 119 (2017) 163401, https://doi.org/10.1103/PhysRevLett.119.163401.
[43] R. Ullah, E. Artacho, A.A. Correa, Core electrons in the electronic stopping of heavy ions, Phys. Rev. Lett. 121 (2018) 116401, https://doi.org/10.1103/PhysRevLett.121.116401.
[44] F. Matias, P.L. Grande, N.E. Koval, J.M.B. Shorto, T.F. Silva, N.R. Arista, Deeper-band electron contributions to stopping power of silicon for low-energy ions, J. Chem. Phys. 161 (2024) 064310, https://doi.org/10.1063/5.0218226.
[45] M.J. Berger, et al., ICRU Report 49: stopping powers and ranges for protons and alpha particles, J. ICRU 25 (1993) 1–68.
[46] H. Bichsel, Stopping power of fast charged particles in heavy elements, National Institute of Standards and Technology (1991) Report NIST IR-4550.
[47] T.D.M. Weijers, B.C. Duck, D.J. O'Connor, The development of a stopping power predictor for ions with energies of 0.1–1.0 MeV/u in elemental targets, Nucl. Instrum. Methods Phys. Res. B 215 (2004) 35, https://doi.org/10.1016/j.nimb.2003.08.027.
[48] K. Wittmaack, Misconceptions impairing the validity of the stopping power tables in the SRIM library and suggestions for doing better in the future, Nucl. Instrum. Methods Phys. Res. B 380 (2016) 57, https://doi.org/10.1016/j.nimb.2016.04.057.
[49] H.H. Andersen, J.F. Ziegler, Hydrogen stopping powers and ranges in all elements (The Stopping and Ranges of Ions in Matter, Vol 3). Pergamon Press, New York, NY, 1st edition, 1977.
[50] The anonymous referee thankfully pointed out that from a theoretical standpoint, at least for metals, the electronic stopping scales as $E^{0.5}$ at extremely low energies. The use of an $E^{0.45}$ dependence should be interpreted as describing a transition regime from extremely low to low energies.
[51] C. Varelas, J. Biersack, Reflection of energetic particles from atomic or ionic chains in single crystals, Nucl. Instrum. Methods 79 (1970) 213, https://doi.org/10.1016/0029-554X(70)90141-2.
[52] J.F. Ziegler, Helium stopping powers and ranges in all elements. The Stopping and Ranges of Ions in Matter, 1st edition,, Pergamon Press, New York, NY, 1977.
[53] W. Brandt, M. Kitagawa, Effective stopping-power charges of swift ions in condensed matter, Phys. Rev. B 25 (1982) 5631, https://doi.org/10.1103/PhysRevB.25.5631.
[54] J.F. Ziegler, J.P. Biersack, M.D. Ziegler, SRIM – the stopping and range of ions in matter, SRIM Co., Chester, ML, version v05, 2008. ISBN: 0-9654207-1-X.
[55] J.F. Ziegler, M.D. Ziegler, J.P. Biersack, SRIM – the stopping and range of ions in matter (2010), Nucl. Instrum. Methods Phys. Res. B 268 (2010) 1818, https://doi.org/10.1016/j.nimb.2010.02.091.
[56] H. Paul, Comparing experimental stopping power data for positive ions with stopping tables, using statistical analysis, Nucl. Instrum. Methods in Phys. Research B 273 (2012) 15, https://doi.org/10.1016/j.nimb.2011.07.026.
[57] H. Paul, Stopping power database, available at https:/www-nds.iaea.org/stopping/ (accessed August 15, 2023); IAEA Stopping Power Database, version 2023-11, https://nds.iaea.org/stopping/ (accessed Dec. 12, 2025).
[58] C.C. Montanari, P. Dimitriou, The IAEA stopping power database, following trends in stopping power of ions in matter, Nucl. Instrum. Methods Phys. Res. B 408 (2017) 50, https://doi.org/10.1016/j.nimb.2017.03.138.
[59] International Atomic Energy Agency (IAEA). Improvement of the Reliability and Accuracy of Heavy Ion Beam Analysis. Technical Reports Series No. 485, IAEA, Vienna, 2019. ISBN 978-92-0-103517-2; https://www.iaea.org/publications/11130/ (accessed Dec. 12, 2025).
[60] N.P. Barradas, C. Jeynes, R.P. Webb, Simulated annealing analysis of Rutherford backscattering data, Appl. Phys. Lett. 71 (1997) 291, https://doi.org/10.1063/1.119524.
[61] M. Mayer, SIMNRA IPP 9/113, Max-Planck-Institut für Plasmaphysik, Garching, Germany, 1997.
[62] M. Mayer, SIMNRA, a Simulation Program for the Analysis of NRA, RBS and ERDA, Proceedings of the 15th International Conference on the Application of Accelerators in Research and Industry, J.L. Duggan and I.L. Morgan (eds.), American Institute of Physics Conference Proceedings 475 (1999) 541; doi: 10.1063/1.59188.
[63] R. Heller, N. Klingner, N. Claessens, C. Merckling, J. Meersschaut, Differential evolution optimization of Rutherford backscattering spectra, J. Appl. Phys. 132 (2022) 165302, https://doi.org/10.1063/5.0096497.
[64] G.G. Marmitt, Metal oxides of resistive memories investigated by electron and ion backscattering, PhD. thesis, Universidade Federal do Rio Grande do Sul (2017) 74 pp, URL: hdl.handle.net/10183/170451.
[65] F. Schiettekatte, Fast Monte Carlo for ion beam analysis simulations, Nucl. Instrum. Methods Phys. Res. B 266 (2008) 1880, https://doi.org/10.1016/j.nimb.2007.11.075.
[66] K. Arstila, J. Julin, M.I. Laitinen, J. Aalto, T. Konu, S. Kärkkäinen, S. Rahkonen, M. Raunio, J. Itkonen, J.-P. Santanen, T. Tuovinen, T. Sajavaara, Potku – New analysis software for heavy ion elastic recoil detection analysis, Nucl. Instrum. Methods Phys. Res. B 331 (2014) 34, https://doi.org/10.1016/j.nimb.2014.02.016.
[67] A. Mutzke, W. Eckstein, R. Dohmen, K. Schmid, U. von Toussaint, R. Schneider, G. Bandelow, SDTrimSP Version 6.00. https://doi.org/10.17617/2.3026474.
[68] F. Matias, T.F. Silva, N.E. Koval, J.J.N. Pereira, P.C.G. Antunes, P.T.D. Siqueira, M.H. Tabacniks, H. Yoriyaz, J.M.B. Shorto, P.L. Grande, Efficient computational modeling of electronic stopping power of organic polymers for proton therapy optimization, Sci. Rep. 14 (2024) 9868, https://doi.org/10.1038/s41598-024-60651-0.
[69] Y.G. Li, Y. Yang, P.P. Short, Z.J. Ding, Z. Zeng, J. Li, IM3D: a parallel Monte Carlo code for efficient simulations of primary radiation displacements and damage in 3D geometry, Sci. Rep. 5 (2015) 18130, https://doi.org/10.1038/srep18130.
[70] W.A. Parfitt, R.B. Jackman, Nucl. Inst. Methods Phys. Res. B 478 (2020) 21, https://doi.org/10.1016/j.nimb.2020.05.015.
[71] X. Guo, H. Wang, C. Li, S. Zhao, K. Jin, J. Xue, Development of an electronic stopping power model based on deep learning and its appl in ion range prediction, Chin. Phys. B 31 (2022) 073402, https://doi.org/10.1088/1674-1056/ac4e0c.
[72] F. Bivort Haiek, A.M.P. Mendez, C.C. Montanari, D.M. Mitnik, ESPNN a novel electronic stopping power neural network code built on the IAEA stopping power database, J. Appl. Phys. 132 (2022) 245103, https://doi.org/10.1063/5.0130875.
[73] F. Akbari, S. Taghizadeh, D. Shvydka, N.N. Sperling, E.I. Parsai, Predicting electronic stopping powers using stacking ensemble machine learning method, Nucl. Instrum. Methods Phys. Res. B 538 (2023) 8, doi:10.1063/ j. nimb.2023.02.023.
[74] F. Cheng, X. Liu, Q. Zheng, C. Zhang, B. Da, Y. Li, Machine learning study of universal electronic stopping cross-sections of ions in matter, Nucl. Eng. Technol. 57 (2025) 103271, https://doi.org/10.1016/j.net.2024.10.033.
[75] N.P. Barradas, C. Jeynes, R.P. Webb, E. Wendler, Accurate determination of the stopping power of 4He in Si using Bayesian inference, Nucl. Inst. Methods Phys. Res. B 194 (2002) 15–25, https://doi.org/10.1016/S0168-583X(02)00494-9.
[76] A.J.M. Plompen, F. Munnik, J. Raïsänen, U. Wätjen, Stopping powers of 200 - 3200 keV He and p in polyimide, J. Appl. Phys. 80 (1996) 3147, https://doi.org/10.1063/1.363277.
[77] G. Konac, Ch. Klatt, S. Kalbitzer, Universal fit formula for electronic stopping of al ions in carbon and silicon, Nucl. Instrum. Methods Phys. Res. B 146 (1998) 106, https://doi.org/10.1016/S0168-583X(98)00453-4.
[78] G. Konac, S. Kalbitzer, Ch. Klatt, D. Niemann, R. Stoll, Energy loss and straggling of H and He ions of keV energies in Si and C, Nucl. Instrum. Methods Phys. Res. B 136 (1998) 159, https://doi.org/10.1016/S0168-583X(98)80016-5.
[79] J. Meersschaut, S. Meersschaut, J.-P. Soulié, R. Heller, Electronic stopping cross section for He in Ru, derived from RBS spectra, Nucl. Instrum. Methods Phys. Res. B 553 (2024) 165406, https://doi.org/10.1016/j.nimb.2024.165406.
[80] P. Virtanen, R. Gommers, et al., SciPy 1.0: fundamental algorithms for scientific computing in Python, Nat. Methods 17 (2020) 261, https://doi.org/10.1038/s41592-019-0686-2.
[81] H. Paul, The solid–gas difference in stopping powers, and statistical analysis of stopping power data, Nucl. Instrum. Methods B 267 (2009) 9, https://doi.org/10.1016/j.nimb.2008.10.065.

[82] M.J. Berger et al., Stopping power and range tables for electrons, protons and helium ions, https://www.nist.gov/pml/stopping-power-range-tables-electrons-protons-and-helium-ions (accessed Dec. 12, 2025), https://doi.org/10.18434/T4NC7P.
[83] J.P. Biersack, L.G. Haggmark, A Monte-Carlo computer program for the tranport of energetic ions in amorphous targets, Nucl. Instrum. Methods 174 (1980) 257, https://doi.org/10.1016/0029-554X(80)90440-1.
[84] J.F. Ziegler, J.M. Manoyan, The stopping of ions in compounds, Nucl. Instrum. Methods in Phys. Res B 35 (1988) 215, https://doi.org/10.1016/0168-583X(88)90273-X.
[85] E. Rauhala, J.F. Ziegler, Chapter 2 in J.R. Tesmer, M. Nastasi, Eds. Handbook of Modern Ion Beam Materials Analysis. Materials Research Society, Pittsburgh, Pennsylvania, 1995.
[86] M. Mayer, Improved physics in SIMNRA 7, Nucl. Instrum. Methods Phys. Res. Sect. B 332 (2014) 176, https://doi.org/10.1016/j.nimb.2014.02.056.
[87] N.P. Barradas, C. Jeynes, Advanced physics and algorithms in the IBA DataFurnace, Nucl. Instrum. Methods Phys Res. B 266 (2008) 1875, https://doi.org/10.1016/j.nimb.2007.10.044.
[88] K. Arstila, T. Sajavaara, J. Keinonen, Monte Carlo simulation of multiple and plural scattering in elastic recoil detection, Nucl. Instrum. Methods in Physics Res. B 174 (2001) 163, https://doi.org/10.1016/S0168-583X(00)00435-3.
[89] J.F. Ziegler, SRIM-2013.00 http://www.srim.org/SRIM/SRIMLEGL.htm (accessed Jan. 1, 2025).
[90] J.F. Ziegler, J.P. Biersack, M.D. Ziegler, SRIM 2008. http://www.srim.org (accessed Jan. 1, 2025).
[91] D. Jedrejcic, U. Greife, Energy loss of low energy H and He ions in light gases, Nucl. Instrum. Methods Phys. Res. B 428 (2018) 1–8, https://doi.org/10.1016/j.nimb.2018.04.039.
[92] P. Grande, G. Schiwietz, Nonperturbative stopping-power calculation for bare and neutral hydrogen incident on He, Phys. Rev. A 47 (1993) 1119, https://doi.org/10.1103/PhysRevA.47.1119.
[93] J.F. Ziegler, W.K. Chu, J.S.-Y. Feng, Empirical corrections to the energy loss of ^{4}He ions in oxides, Appl. Phys. Lett. 27 (1975) 387, https://doi.org/10.1063/1.88503.
[94] A.M.P. Mendez, GitHub account, https://github.com/ale-mendez/ESPNN, (accessed Nov. 30, 2025).
[95] N.P. Barradas, K. Arstila, G. Battistig, M. Bianconi, N. Dytlewski, C. Jeynes, E. Kótai, G. Lulli, M. Mayer, E. Rauhala, E. Szilágyi, M. Thompson, International Atomic Energy Agency intercomparison of ion beam analysis software, Nucl. Instrum. Methods Phys. Res. B 262 (2007) 281, https://doi.org/10.1016/j.nimb.2007.05.018.
[96] T.T. Tran, L. Jablonka, B. Bruckner, S. Rund, D. Roth, M.A. Sortica, P. Bauer, Z. Zhang, D. Primetzhofer, Electronic interaction of slow hydrogen and helium ions with nickel-silicon systems, Phys. Rev. A 100 (2019) 032705, https://doi.org/10.1103/PhysRevA.100.032705.
[97] A. Javanainen, M. Sillanpää, W.H. Trzaska, A. Virtanen, G. Berger, W. Hajdas, R. Harboe-Sørensen, H. Kettunen, T. Malkiewicz, M. Mutterer, J. Perkowski, A. Pirojenko, I. Riihimäki, T. Sajavaara, G. Tyurin, H.J. Whitlow, Experimental linear energy transfer of heavy ions in silicon for RADEF cocktail species, IEEE Trans. Nucl. Sci. 56 (2009) 2242, https://doi.org/10.1109/TNS.2008.2009983.
[98] P.R. Bevington, D.K. Robinson, Data reduction and error analysis for the physical sciences. McGraw-Hill international editions: Physics series, McGraw-Hill, New York, 2003.
[99] D.I. Thwaites, Current status of physical state effects on stopping power, Nucl. Instrum. Methods Phys. Res., B 12 (1985) 84, https://doi.org/10.1016/0168-583X(85)90705-0.
[100] F. Matias, N.E. Koval, P. de Vera, R. Garcia-Molina, I. Abril, J.M.B. Shorto, H. Yoriyaz, J.J.N. Pereira, T.F. Silva, M.H. Tabacniks, M. Vos, P.L. Grande, Stopping cross sections for protons across different phases of water, Phys. Rev. Lett. 135 (2025) 148003, https://doi.org/10.1103/ksdx-mnd7.
[101] N. Catarino, E. Alves, L.C. Alves, J. Flora, M. Peres, R.C. Silva, N.P. Barradas, Stopping power determination of ^{4}He and ^{1}H in Sc, Gd and Yb using bulk sample method, Nucl. Instrum. Methods Phys. Res., B 572 (2026) 166005, https://doi.org/10.1016/j.nimb.2026.166005.
[102] E. Ntemou, S. Lohmann, R. Holenák, D. Primetzhofer, Electronic interaction of slow hydrogen, helium, nitrogen, and neon ions with silicon, Phys. Rev. B 107 (2023) 155145; https://doi.org/10.1103/PhysRevB.107.155145; Erratum, Phys. Rev. B 109 (2024) 239902; https://doi.org/10.1103/PhysRevB.109.239902.